J. Fluid Mech. (2001), *vol.* 433, *pp.* 1–27. Printed in the United Kingdom

Dynamics of pancake-like vortices in a stratified fluid: experiments, model and numerical simulations

By M. BECKERS[1], R. VERZICCO[2], H. J. H. CLERCX[1] AND G. J. F. VAN HEIJST[1]

[1] J. M. Burgers Centre, Fluid Dynamics Laboratory, Department of Physics, Eindhoven University of Technology, PO Box 513, 5600 MB Eindhoven, The Netherlands

[2] Politecnico di Bari, Dipartimento di Ingegneria Meccanica e Gestionale, Via Re David 200, 70125 Bari, Italy.

(Received 18 June 1998 and in revised form 17 July 2000)

The dynamics and the three-dimensional structure of vortices in a linearly stratified, non-rotating fluid are investigated by means of laboratory experiments, an analytical model and through numerical simulations. The laboratory experiments show that such vortices have a thin pancake-like appearance. Due to vertical diffusion of momentum the strength of these vortices decreases rapidly and their thickness increases in time. Also it is found that inside a vortex the linear ambient density profile becomes perturbed, resulting in a local steepening of the density gradient. Based on the assumption of a quasi-two-dimensional axisymmetric flow (i.e. with zero vertical velocity) a model is derived from the Boussinesq equations that illustrates that the velocity field of the vortex decays due to diffusion and that the vortex is in so-called cyclostrophic balance. This means that the centrifugal force inside the vortex is balanced by a pressure gradient force that is provided by a perturbation of the density profile in a way that is observed in the experiments. Numerical simulations are performed, using a finite difference method in a cylindrical coordinate system. As an initial condition the three-dimensional vorticity and density structure of the vortex, found with the diffusion model, are used. The influence of the Froude number, Schmidt number and Reynolds number, as well as the initial thickness of the vortex, on the evolution of the flow are investigated. For a specific combination of flow parameters it is found that during the decay of the vortex the relaxation of the isopycnals back to their undisturbed positions can result in a stretching of the vortex. Potential energy of the perturbed isopycnals is then converted into kinetic energy of the vortex. However, when the stratification is strong enough (i.e. for small Froude numbers), the evolution of the vortex can be described almost perfectly by the diffusion model alone.

1. Introduction

Coherent vortex structures are characteristic features of stratified flows. In the context of oceanography and meteorology, Meddies formed by salty water flowing from the Mediterranean Sea into the Atlantic Ocean (Bower, Armi & Ambar 1997), and high and low pressure cells in the atmosphere are only two typical examples. In many laboratory studies it has been shown that decaying turbulence in a stratified fluid, generated by moving rakes, grids or bluff bodies, eventually results in the formation of a large number of flat pancake-like vortex structures, that by mutual

interaction increase in size and decrease in number. Due to the quasi-two-dimensional (Q2D) nature of the flow in a strongly stratified fluid, the organization of stratified turbulence into coherent vortex structures appears to have some analogies with the process of self-organization in purely two-dimensional flows, see McWilliams (1984). However, an important difference is the fact that vortices in a stratified fluid essentially have a three-dimensional structure.

The vertical structure of vortices in a stratified fluid has so far only been studied for arrays of vortices that arise in the far wake of a sphere towed through a linearly stratified fluid, see Pao & Kao (1977), Chomaz *et al.* (1993) and Spedding, Browand & Fincham (1996), and for freely decaying stratified grid turbulence, see Fincham, Maxworthy & Spedding (1996). The latter authors proposed a model for the vorticity structure of the Q2D vortices in such a wake. The vortex lines in these structures form connections between different vortices at different levels in the fluid, and eventually reconnect to form closed loops. A similar model has been suggested by Pao & Kao (1977) for the vortices in the wake of a sphere in a stratified fluid. The decay of dipolar vortices in a stratified fluid due to diffusion of vorticity in a direction perpendicular to the flow field was described by Flór, van Heijst & Delfos (1995). Several models were studied by the authors to describe this vertical diffusion process. These models were extended by Trieling & van Heijst (1998) to include also radial diffusion for the case of monopolar vortices. In both studies extensive experimental effort has been made to measure fluid motion in the vortex symmetry plane. However, these measurements only provide information on the decay rate of the vortex, not on the actual vertical structure.

The vorticity distribution of a single vortex in a stratified fluid has not yet been investigated in detail. This apparently very simple case is particularly interesting, because the vortex lines need to form closed loops inside the fluid, but in contrast to the vortex wake behind a sphere or a grid only one vorticity structure is present. The investigation of the structure of a single vortex in a linearly stratified fluid can be a convenient starting point to gain a better understanding of the interactions between and the structure of the vortices that result from decaying turbulence in a stratified medium. Furthermore, knowledge of the structure of a single axisymmetric vortex will be expanded in the future to describe the formation of a so-called tripolar vortex from an unstable monopole in a stratified fluid (see also Flór & van Heijst 1996) and the interaction process between shielded oppositely signed monopoles (see also Schmidt *et al.* 1998). The study of interactions between vortices at different levels in the fluid will then be a next step to understanding the late stages of stratified turbulence.

Two mechanisms that determine the dynamics of axisymmetric vortices in a linearly stratified fluid will be considered here in more detail: radial and vertical diffusion of vorticity and the perturbation of the isopycnals (i.e. the modification of the density distribution inside the vortex). The role of density in the dynamics of a single vortex has been recognized by Flór & van Heijst (1996). They roughly estimated the strength of the perturbation of isopycnals for a vortex, based on the fact that the vortex is in so-called *cyclostrophic balance*, but they did not support this with experimental evidence. Only very recently have density measurements inside vortices (in the far wake of a sphere towed through a stratified fluid) been reported by Bonnier, Eiff & Bonneton (1999). They observed that isopycnals (i.e. planes of constant density) are indeed depressed above the vortex and elevated below the vortex, suggesting that the vortices are in cyclostrophic balance. Furthermore, they found that an identical density structure could be measured for far-wake vortices originating from either

laminar or turbulent near wakes. This suggests that the specific density structure is fairly universal for Q2D vortices in a stratified fluid.

In this paper a model is proposed that describes the motion of an axisymmetric vortex in a linearly stratified fluid, and the vorticity and density distribution of this vortex will be derived. The model starts with the assumption that there is only an azimuthal velocity component with a Gaussian distribution in the vertical direction. It is then found that it is necessary to modify the initially linear density profile inside the vortex in order to maintain the swirling motion. The model is compared with results from both laboratory experiments and numerical simulations, in order to assess the validity of the assumptions. The paper is organized as follows: in the following section the experimental and numerical techniques are briefly summarized. Experimental observations are described in § 3, and then in § 4 a model to interpret the observations is introduced. In § 5 the results of several numerical simulations are shown and discussed to verify the model accuracy and its limitations. Conclusions are given in § 6. A short Appendix is added with details of the solution of the diffusion model.

2. Investigation methods

The structure of pancake-like isolated monopolar vortices in a stratified fluid is investigated by laboratory experiments and numerical simulations. The combined use of these different approaches allows the flow dynamics to be studied for a wide range of parameters and the results of each technique to be checked against each other. In the following the main features of the techniques are described, while for more detailed descriptions the reader is referred to the cited literature.

2.1. *Experimental setup and measurement techniques*

The experiments are performed in a square tank of size $80 \times 80 \times 40\,\mathrm{cm}^3$ filled with a linearly salt-stratified fluid. A sketch of the experiment tank is given in figure 1(*a*). The density stratification is constructed by the *two-tank method*, described in detail by Fortuin (1960) and Oster & Yamamoto (1963). To obtain quantitative information on the velocity field of the vortex, small polystyrene particles (of about 1 mm in diameter) are added to the stratification and they float at their neutrally buoyant level in the fluid. These tracer particles are illuminated from the side by a light sheet, produced by slide projectors. The thickness of this light sheet is typically of the order of 5 mm. Above the tank a video camera is mounted, by which the particle motions are recorded on video tape.

Vortices are generated by means of the so-called *tangential injection method* (Flór & van Heijst 1996). Fluid with matched density is injected horizontally along the inner wall of a bottomless thin-walled cylinder, which is positioned in the fluid at the same level as the tracer particles (figure 1*b*). An amount of fluid ΔV is injected during a period Δt at an injection rate defined by $Q = \Delta V/\Delta t$. The injection results in a circular flow inside the cylinder, and a discus-like vortex is released when the cylinder is carefully removed by lifting it out of the fluid. During this removal care should be taken that the cylinder is moved vertically in order to prevent the vortex just created from becoming vertically sheared by motion induced at other levels. The removal should also be very slow, in order to prevent the generation of internal waves. As the present investigation only focuses on the dynamics of Q2D vortices, the details of the flow shortly after removing the cylinder are not discussed here. The density stratification of the fluid eventually ensures the two-dimensional character of the flow

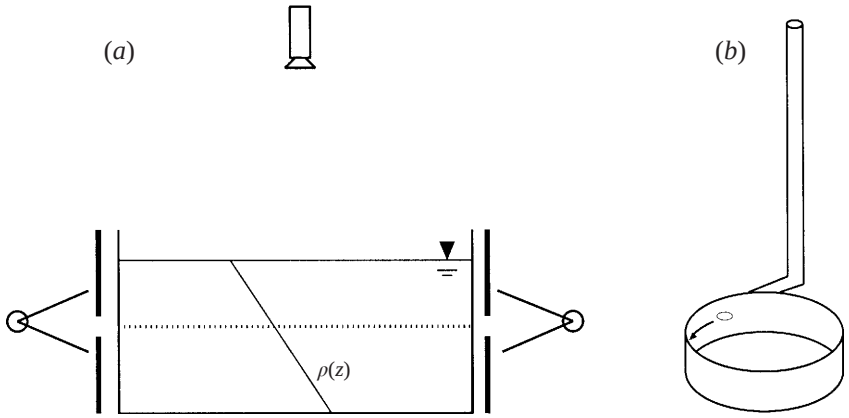

FIGURE 1. (*a*) Schematic representation of the experiment tank. Tracer particles float at approximately half the fluid depth and they are illuminated from the sides by two light sheets, produced by slide projectors. Above, a video camera is mounted that records the particle motion on video tape. (*b*) Device used in the laboratory experiments to generate a monopolar vortex by the 'tangential injection method'.

inside the vortex, and possible disturbances created during the removal of the cylinder are first allowed to die away, before the flow is analysed. For convenience the time $t = 0$ is chosen as the moment when the fluid injection is stopped. For the reasons described above the first velocity measurements are generally not taken until $t \approx 20$ s.

After the experiments the video tape with the particle motions, see figure 2(*a*), is processed with the *DigImage* system, developed by Dalziel (1992), to determine the horizontal velocity field of the vortex at the symmetry plane, see figure 2(*b*). The velocity field found by the two-dimensional particle tracking procedure (in which particles are located at arbitrary positions in the plane of motion) is then interpolated onto a rectangular grid (figure 2*c*) after which the vorticity component normal to the plane is computed by differentiation (figure 2*d*).

During the experiments density measurements are also performed by using a conductivity probe (see Davies 1992). The probe is mounted on a traversing mechanism that moves it vertically through the stratification at a typical speed of 6–8 cm s^{-1}. The traversing mechanism is driven by a step motor which is controlled by a personal computer. During the movement of the probe its output is sampled at a rate of 100 Hz; the density measurements thus result in an almost continuous relationship between the fluid depth z and the density $\rho(z)$. The local buoyancy frequency N of the fluid is then easily determined by calculating the density gradient: $N^2(z) = -(g/\rho)\,\mathrm{d}\rho/\mathrm{d}z$.

2.2. *Numerical simulations*

In addition to the laboratory experiments, numerical simulations are performed based on the time-dependent incompressible Navier–Stokes equations. The numerical code, developed by Verzicco & Orlandi (1996), is adapted to enable the simulation of flows in a linearly stratified fluid as described in the following. The equations are first written in the Boussinesq approximation; this assumption is suggested by the observation that for these flows, in nature as well as in laboratory experiments, the relative density variation rarely reaches the value of a few percent of the reference density. Furthermore, the approximation simplifies the equations of motion considerably.

The Boussinesq approximation implies that the fluid density (ρ) and pressure (p) can be expanded around a homogeneous basic state at rest (i.e. with $\boldsymbol{v} = 0$) with fluid

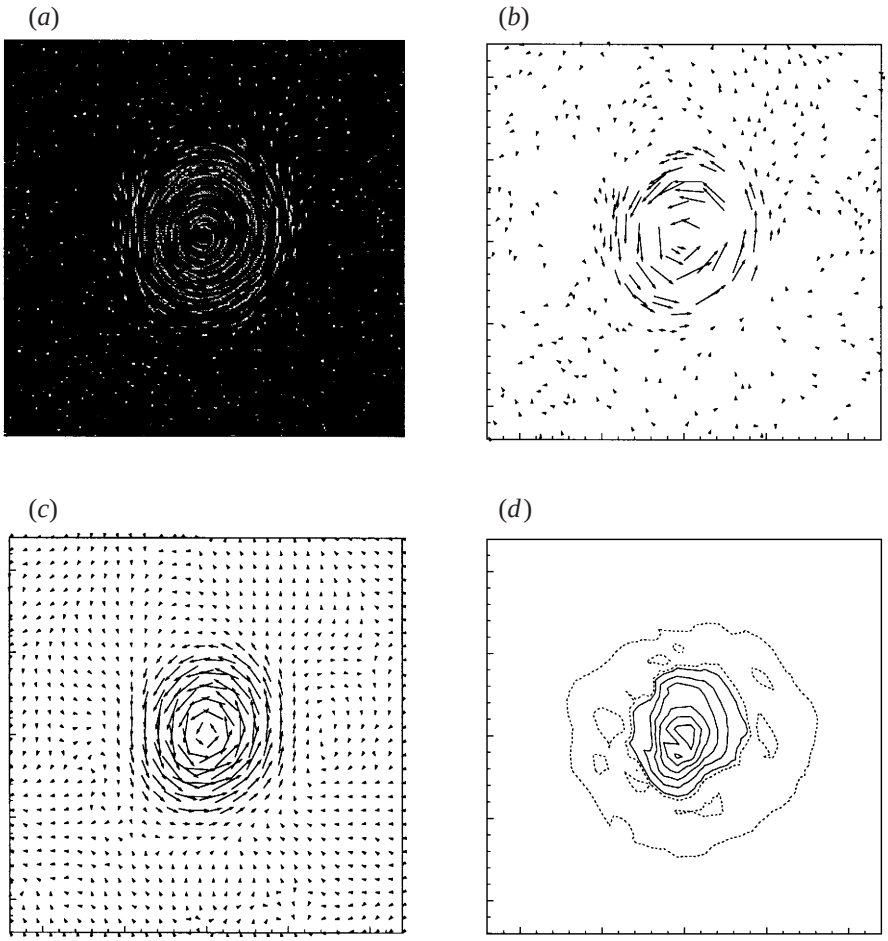

FIGURE 2. (*a*) 'Streaks' formed by moving particles obtained in a particle tracking experiment. (*b*) Velocity field found by following the tracer particles in time. (*c*) Interpolated velocity field on a grid of 30×30 points. (*d*) Contour plot of the (vertical) vorticity distribution.

density ρ_0 and pressure $p_0(z)$. The differences between the pressure and density and that basic state are then written as a part that represents a linear density profile $\bar{\rho}(z)$ with the pressure distribution $\bar{p}(z)$, which is in hydrostatic balance, and a deviation from the linear density profile, indicated by a tilde:

$$p(\boldsymbol{x}, t) = p_0(z) + \bar{p}(z) + \tilde{p}(\boldsymbol{x}, t), \tag{2.1}$$

$$\rho(\boldsymbol{x}, t) = \rho_0 + \bar{\rho}(z) + \tilde{\rho}(\boldsymbol{x}, t). \tag{2.2}$$

The governing equations for the perturbation field $(\boldsymbol{v}, \tilde{\rho}, \tilde{p})$ are then put in a non-dimensional form (omitting symbols that indicate the non-dimensional character of the variables) by scaling the velocities by a typical velocity scale V, lengths by a typical length scale L, pressure by $\rho_0 V^2$ and density by $N^2 L \rho_0 / g$ (with g the gravity acceleration) and read

$$\frac{\partial \boldsymbol{v}}{\partial t} + (\boldsymbol{v} \cdot \nabla)\boldsymbol{v} = -\nabla \tilde{p} - \frac{1}{F^2}\tilde{\rho}\boldsymbol{e}_z + \frac{1}{Re}\nabla^2 \boldsymbol{v}, \tag{2.3}$$

$$\nabla \cdot \boldsymbol{v} = 0, \tag{2.4}$$

$$\frac{\partial \tilde{\rho}}{\partial t} + (\boldsymbol{v} \cdot \nabla)\tilde{\rho} - v_z = \frac{1}{ScRe}\nabla^2 \tilde{\rho}, \tag{2.5}$$

with $\boldsymbol{e}_z$ the unit vector pointing vertically upward (with an orientation opposite to gravity) and $v_z = \boldsymbol{v} \cdot \boldsymbol{e}_z$ the velocity component in that direction. The variables F, Re and Sc are the Froude, Reynolds and Schmidt numbers, respectively, defined as $F = V/(LN)$, $Re = VL/\nu$ and $Sc = \nu/\kappa$ with ν the kinematic viscosity, κ the diffusivity of salt in water and N the buoyancy frequency defined as $N^2 = -(g/\rho_0)\,\mathrm{d}\bar{\rho}/\mathrm{d}z$. The typical velocity and length scales V and L will be defined later on.

Equations (2.3)–(2.5), written in cylindrical coordinates and discretized by central second-order finite-difference approximations on a staggered grid, are solved by a fractional-step method whose features are described in Verzicco & Orlandi (1996). The pressure and density are defined at the centres of the computational cells, whereas the different velocity components are defined at the centres of the cell boundaries that are perpendicular to the directions in which the velocities point. In a cylindrical coordinate system, with velocity components (v_r, v_θ, v_z), singularities can arise in the equations of motion at $r = 0$. The only velocity component, however, that is evaluated at this position is v_r. The problem can therefore be overcome by defining the variable $q_1 = v_r r$ instead, which simplifies the discretization as $q_1 = 0$ at $r = 0$. The other variables are then $q_2 = v_\theta$ and $q_3 = v_z$.

The equations of motion for $\boldsymbol{q}$ are discretized in time, where the nonlinear (advective) and buoyancy terms are calculated explicitly by using a *third-order Runge–Kutta* scheme, and the discretization of the viscous term implicitly by using a *Crank–Nicolson* technique. The time-advancement of the numerical scheme is thus second-order accurate in time, i.e. $\mathcal{O}(\Delta t)^2$, and uses a so-called *fractional-step* method, which consists of four steps. (1) The velocity field $\boldsymbol{q}^{(m+1)}$ at the new timestep $(m+1)$ is approximated by $\hat{\boldsymbol{q}}$ by using the pressure gradient $\nabla p^{(m)}$ from the previous timestep. This approximation for the pressure gradient introduces an error in the velocity field, that can be accounted for by the introduction of (the gradient of) a scalar quantity, i.e. $\nabla \Phi = \alpha(\boldsymbol{q}^{(m+1)} - \hat{\boldsymbol{q}})$, where α is a constant of proportionality. (2) Φ can be obtained from the Poisson equation that results by applying the conservation of mass to the new velocity field $\nabla^2 \Phi = \alpha \nabla \cdot \hat{\boldsymbol{q}}$, because $\boldsymbol{q}^{(m+1)}$ should be divergence-free. As $\boldsymbol{q}^{(m+1)}$ and $\hat{\boldsymbol{q}}$ both satisfy the same conditions at the wall, the necessary boundary condition to solve the Poisson equation is given by $\nabla \Phi = 0$. (3) Substitution of Φ and $\hat{\boldsymbol{q}}$ in the equation mentioned in step (1) yields the correct velocity field $\boldsymbol{q}^{(m+1)}$ at the new timestep. (4) Finally, the correct pressure $p^{(m+1)}$ at the new timestep can be calculated by the substitution of the correct velocity field $\boldsymbol{q}^{(m+1)}$ in the equations of motion. An extensive description of the time-advancement procedure and the spatial discretizations of all terms in the equations of motion (in cylindrical coordinates) is given by Verzicco & Orlandi (1996).

The flow in the simulations has periodic boundary conditions in the azimuthal direction. In this paper the flow is assumed to remain axisymmetric during its evolution and the three-dimensional numerical scheme (r, θ, z) can conveniently be used in a two-dimensional way (r, z) by taking all derivatives in the azimuthal direction to be zero, thereby saving computational time. All the simulations are run in a domain of radial and vertical dimensions $L_r = 8L$ and $L_z = 8L$, each direction discretized by 128 gridpoints. In the vertical direction periodic boundary conditions are used while the lateral wall is assumed stress-free. It is checked by runs with bigger L_r and L_z that the finiteness of the computational domain does not affect the results. Similarly,

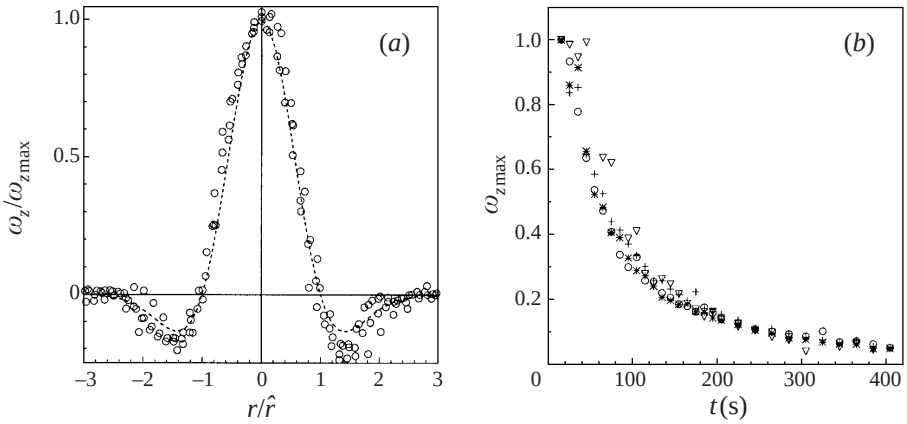

FIGURE 3. (*a*) Typical cross-section of the vorticity field of a monopole. The dashed line represents the vorticity profile for $\alpha = 2$. (*b*) Decay of the maximum values of the vorticity (normalized by their values at $t = 20\,\mathrm{s}$) of a monopolar vortex in four similar experiments, performed under equal conditions: $Q = 2.22\,\mathrm{cm^3\,s^{-1}}$, $\Delta V = 50\,\mathrm{cm^3}$ and $N = 1.9\,\mathrm{rad\,s^{-1}}$.

the grid independence is verified by simulating some cases on a 256×256 grid and even a 512×512 grid and again the results prove to be indistinguishable.

3. Experimental observations

In this investigation the velocity (and vorticity) distribution inside a monopolar vortex is studied. First the results of some laboratory experiments are discussed. Later these results will be used to define the initial conditions for a vortex model and for the numerical simulations.

Figure 3(*a*) shows an azimuthally averaged radial cross-section of the vorticity at the symmetry plane ($z = 0$) of a typical monopole. In agreement with previous results by Flór & van Heijst (1996) and Trieling & van Heijst (1998), the circular vortex has a core of one sign of vorticity surrounded by a ring of oppositely signed vorticity. The vorticity profile is well fitted by the so-called α-profile introduced by Carton, Flierl & Polvani (1989): $\omega_z(r) = (1 - 1/2\alpha r^\alpha)\exp(-r^\alpha)$, with a value of α that for this generation process is always around 2.† The presence of this ring is explained by the fact that vortex lines should make closed loops inside the fluid, as the vortex is created at a sufficient distance from both the bottom of the tank and the surface of the fluid: vortex lines directed upwards in the core of the vortex should therefore point downwards in another region of the fluid, resulting in the presence of a ring of oppositely signed vertical vorticity. To investigate the reproducibility of the monopoles generated, the decay of the maximum vorticity in the plane of symmetry is measured as a function of time for four experiments. The results are shown in figure 3(*b*) and, although some scatter is observed, the intensity and the time scale of the decay is found to be essentially the same for all vortices.

Figure 4 shows the results of four separate experiments. In each experiment a vortex is created at a different level in the stratification, such that in every experiment

† The reason that the vorticity profile of the vortex agrees so well with the α-profile for $\alpha = 2$ is due to radial diffusion working on an isolated circular (two-dimensional) vortex. This process is described by Kloosterziel (1990) and Beckers *et al.* (1999) and will be discussed in more detail in a future publication.

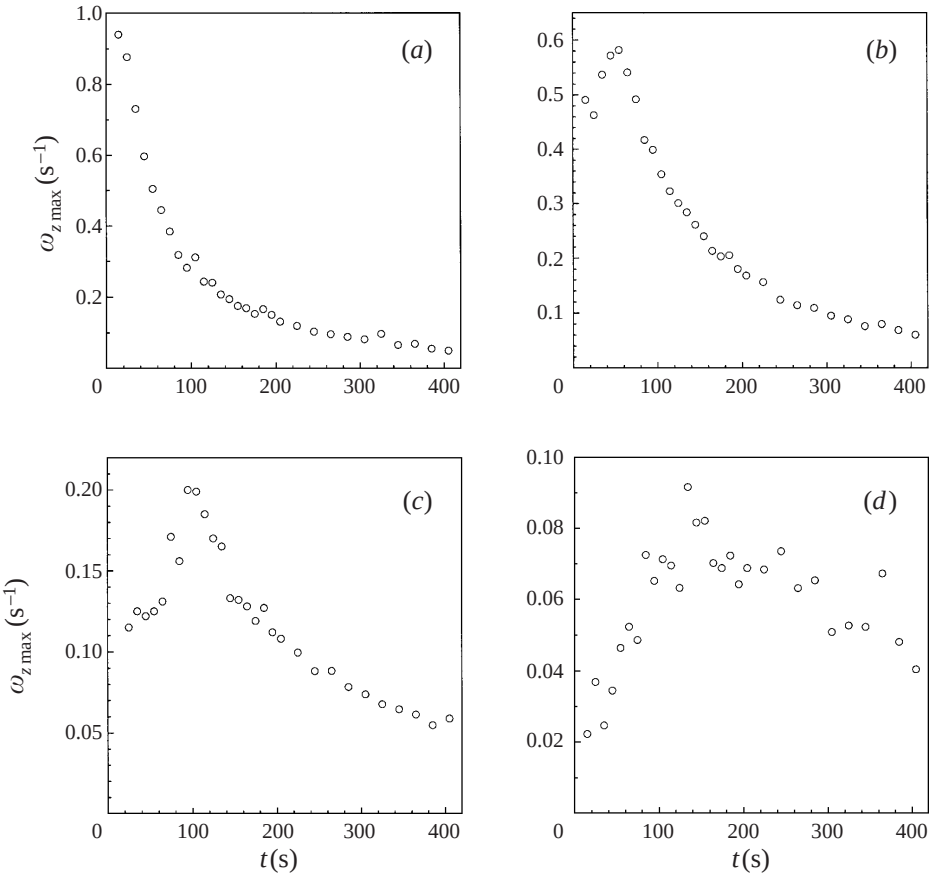

FIGURE 4. Evolution of the maximum values of the vorticity of a monopolar vortex in four similar experiments. In each experiment the flow field is measured at a different level in the vortex. The vortices have all been created under equal experimental conditions (see caption of figure 3). The levels are (*a*) $z = 0$ (i.e. the symmetry plane), (*b*) 1.0 cm, (*c*) 2.0 cm and (*d*) 3.0 cm.

the layer of tracer particles is positioned at a different distance from the symmetry plane of the vortex. In this way the flow inside a vortex is measured at four horizontal planes located at different vertical positions: $z = 0$ (i.e. the symmetry plane), 1.0, 2.0 and 3.0 cm, respectively. At $z = 0$, figure 4(*a*), a rapid decay of the maximum vorticity value is observed. In the study by Trieling & van Heijst (1998) it has been shown that this decay can be attributed to vertical diffusion of momentum, or in other words a thickening of the vortex structure. The present measurements of the vorticity at levels other than the symmetry plane of the vortex, figure 4(*b–d*), confirm this finding: the maximum vorticity values at these levels first increase and then decrease. Also the farther the level, at which the vorticity is measured, is away from the symmetry plane, the later the maximum vorticity value at this level attains its peak value. This suggests that the mechanism that causes the decay of the vortex is indeed diffusion of momentum in the vertical direction.

An important question concerns the distribution of the planar flow field in the vertical direction, and consequently the definition of the *thickness* of the vortex. The most obvious vertical distribution of the flow field is Gaussian, because this type of distribution arises naturally when diffusion acts on a layer with initially zero thickness

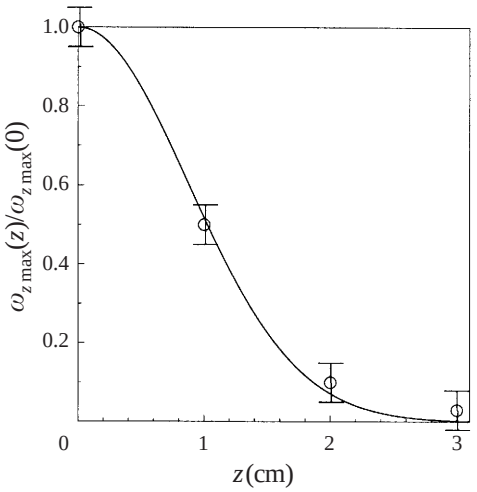

FIGURE 5. Vertical distribution of the maximum values of the vorticity at $t = 20$ s, compared with a Gaussian distribution with $\lambda = 0.9$ cm.

(i.e. a Dirac delta function). In figure 5 an impression of the thickness of the vortex is presented. The maximum vorticity values from the experiments shown in figure 4 at $t = 20$ s are plotted as a function of z and the values compare quite well with a Gaussian distribution given by

$$\omega_{z\,\max} \sim \exp\left(-\frac{z^2}{2\lambda^2}\right), \tag{3.1}$$

where λ is called the thickness of the vortex. The thickness of the distribution shown in figure 5 is $\lambda = 0.9 \pm 0.1$ cm.

To investigate the effect of the vortex on its ambient density distribution, conductivity measurements are performed during the generation and subsequent decay of a vortex (as described in § 2.1). The density profiles are measured through the centre of the vortex before and several times after the injection cylinder is removed and the results are shown in figure 6. In figure 6(*a*) the density profile of the undisturbed fluid is given just before the start of the injection for comparison. Figure 6(*b*) shows the profile at $t = 1$ s, just after stopping the injection, (*c*) at $t = 22$ s and (*d*) at $t = 43$ s. Each dot in the graphs corresponds to one density sample, and the position of the cylinder is marked by the two horizontal dashed lines. The initial density profile is close to linear, and the associated buoyancy frequency is $N = 1.0\,\mathrm{rad\,s^{-1}}$. Just after the injection is stopped, it is clearly observed that the density profile inside the vortex is perturbed; isopycnals are apparently deflected downwards in the upper half of the vortex, and upwards in the lower half. One might object that the mere presence of an injected volume of $50\,\mathrm{cm}^3$ of homogeneous fluid also creates a density anomaly inside the cylinder, because it represents a disk of fluid with a constant density, a radius of 5 cm and a thickness of approximately 0.6 cm. However, such a disk of homogeneous fluid would yield a density anomaly with a buoyancy frequency minimum, in contrast to the density profile shown in figure 6(*b*) that clearly shows a steepening in the density profile and thus a buoyancy frequency maximum. The origin of this density perturbation is investigated in the next section by a simple model for the flow inside a vortex.

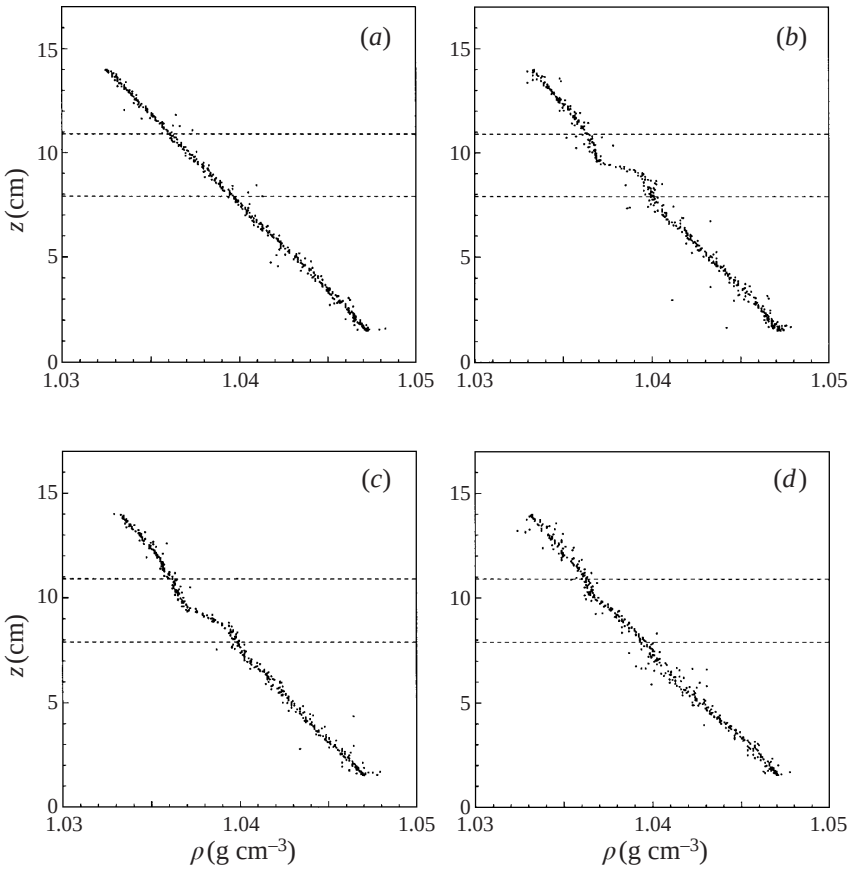

FIGURE 6. Vertical density profiles measured in the centre of a monopolar vortex, at four different times. At $t = 0$ the tangential injection is stopped and at $t = 10\,\mathrm{s}$ the injection cylinder is removed. The profiles are shown (*a*) before the injection, (*b*) just after the injection, but with the cylinder still present, (*c*) at $t = 22\,\mathrm{s}$ and (*d*) at $t = 43\,\mathrm{s}$. The experimental parameters are $Q = 2.22\,\mathrm{cm^3\,s^{-1}}$, $\Delta V = 50\,\mathrm{cm^3}$ and $N = 1.0\,\mathrm{rad\,s^{-1}}$.

4. The diffusion model

In order to understand the results of the laboratory experiments a model is proposed for an axisymmetric vortex in a linearly stratified fluid. This model describes the decay of the vortex due to viscous diffusion only, and is therefore called the *diffusion model*.

Numerical simulations of decaying stratified turbulence by Riley, Metcalfe & Weissman (1981) and Lilly (1983) have shown that for low Froude number (i.e. strongly stratified) flows, the fluid motion can eventually be approximated as Q2D. This means that in a first-order approximation the vertical velocity is zero. Before the measurements were carried out, the vortices in the laboratory experiments were first allowed to adjust after the cylinder was removed. After this adjustment they have laminar flow conditions and they are believed to behave as Q2D. Therefore, consider a Q2D monopolar axisymmetric vortex in a fluid with a stable linear density stratification at a low Froude number. For a convenient analysis of the flow a cylindrical coordinate system is introduced, with r the radial, θ the azimuthal and z the vertical upward coordinate. If, according to the low-F hypothesis, vertical fluid motion is assumed to be absent ($v_z = 0$), and furthermore the flow is assumed to be axisymmetric ($\partial/\partial\theta = 0$),

incompressibility ($\nabla \cdot \boldsymbol{v} = 0$) implies that radial fluid motion is also absent ($v_r = 0$). The three components of equation (2.3) then become

$$-\frac{v_\theta^2}{r} = -\frac{\partial \tilde{p}}{\partial r}, \tag{4.1}$$

$$\frac{\partial v_\theta}{\partial t} = \frac{1}{Re}\left(\frac{\partial^2 v_\theta}{\partial r^2} + \frac{1}{r}\frac{\partial v_\theta}{\partial r} - \frac{v_\theta}{r^2} + \frac{\partial^2 v_\theta}{\partial z^2}\right), \tag{4.2}$$

$$0 = -\frac{\partial \tilde{p}}{\partial z} - \frac{\tilde{\rho}}{F^2}. \tag{4.3}$$

The radial and vertical components of the momentum equation, (4.1) and (4.3), describe the *cyclostrophic* and *hydrostatic* balances, respectively. The azimuthal component is a diffusion equation in two dimensions. Solving the Navier–Stokes equations, satisfying appropriate initial and boundary conditions, yields expressions for the velocity $v_\theta(r, z, t)$, the pressure distribution and the distribution of the density perturbation $\tilde{\rho}$. Once the azimuthal velocity field is known, the vorticity distribution of the Q2D axisymmetric vortex is easily obtained by differentiation:

$$\omega_r = -\frac{\partial v_\theta}{\partial z} \quad \text{and} \quad \omega_z = \frac{1}{r}\frac{\partial (r v_\theta)}{\partial r}. \tag{4.4}$$

It is worth noting that within the hypotheses of the present model the vorticity vector has only radial and vertical components, since the azimuthal component is zero by definition.

Equation (4.2) is solved by the method of separation of variables, details of which are given in the Appendix. Hankel integrals and Fourier transforms are used for the solution, together with the requirements that the solution is finite at the axis ($r = 0$), vanishes for $r \to \infty$ and is symmetric about the vortex midplane. Initial conditions are required to integrate the solution in time and these have been derived from the experimental observations. The initial velocity distribution inside the vortex is assumed to be of the form

$$v_\theta(r, z, 0) = G(r)H(z). \tag{4.5}$$

The vorticity distribution of a monopole in a stratified fluid is characterized by a core of one sign of (vertical) vorticity, surrounded by a ring of oppositely signed vorticity, as shown in the laboratory experiments. For these 'shielded' monopolar vortices the radial distribution of the vertical vorticity in a horizontal plane is well approximated by the α-profile with $\alpha = 2$. Therefore this profile will be used to represent the radial distribution of the velocity distribution, and this gives

$$G(r) = \frac{r}{2}\exp(-r^2). \tag{4.6}$$

The vertical distribution of the azimuthal fluid motion, $H(z)$, is assumed to be Gaussian as was suggested by the experimental observations. The initial vertical distribution is therefore approximated by

$$H(z) = \frac{1}{(2\pi\Lambda^2)^{1/2}}\exp\left(-\frac{z^2}{2\Lambda^2}\right), \tag{4.7}$$

where $\Lambda = \lambda/L$ is a non-dimensional constant, which represents the initial thickness of the vortex.

The time dependence of the velocity distribution can now be computed from (4.2) (see the Appendix for details) and this gives

$$v_\theta(r,z,t) = \frac{r}{2\pi^{1/2}(2\Lambda^2 + (4/Re)t)^{1/2}(1+(4/Re)t)^2} \exp\left(-\frac{z^2}{2\Lambda^2+(4/Re)t}\right) \times \exp\left(-\frac{r^2}{1+(4/Re)t}\right). \quad (4.8)$$

The radial and vertical growth of the vortex, due to diffusion, can be quantified by the temporal evolution of the radial position $\hat{r}(t)$ where the vorticity ω_z changes sign, see (A 12), and by the evolution of the thickness of the vortex, denoted by $\hat{z}(t)$:

$$\hat{r}(t) = \left(1 + \frac{4}{Re}t\right)^{1/2}, \quad (4.9)$$

$$\hat{z}(t) = \left(\Lambda^2 + \frac{2}{Re}t\right)^{1/2}. \quad (4.10)$$

Since the variable r has been non-dimensionalized by the length scale L the expression for $\hat{r}$ shows that L is given by the initial radius of the core of the vortex. Using the expression for the vertical vorticity, see (A 12) in the Appendix, it can be found that the decay of the vortex, based on the maximum value of the vorticity at $r = 0$, is given by

$$\omega_{z\,\max}(z,t) = \frac{1}{\pi^{1/2}(2\Lambda^2 + (4/Re)t)^{1/2}(1+(4/Re)t)^2} \exp\left(-\frac{z^2}{2\Lambda^2+(4/Re)t}\right). \quad (4.11)$$

Since ω is non-dimensionalized by V/L one can find a value for the velocity scale V from $V = (2\pi)^{1/2}\lambda\omega_M$, where ω_M is the experimentally observed (dimensional) initial maximum value of the vorticity, and λ the (dimensional) value for the thickness of the vortex.

By using the cyclostrophic balance (4.1) and the hydrostatic balance (4.3) and eliminating the pressure an expression equivalent to the thermal wind relation for a rotating stratified flow (see, e.g. Pedlosky 1979) is obtained:

$$F^2\frac{2v_\theta}{r}\frac{\partial v_\theta}{\partial z} + \frac{\partial \tilde{\rho}}{\partial r} = 0. \quad (4.12)$$

This equation indicates that a vertical shear of the azimuthal velocity is only possible under the given assumptions if isopycnals (i.e. planes of constant density) are distorted from their equilibrium position, resulting in a non-zero radial density gradient.

It is possible to derive an expression for the density perturbation $\tilde{\rho}(r,z,t)$ that corresponds to a (cyclostrophically balanced) velocity distribution $v_\theta(r,z,t)$ by integration of (4.12). Substitution of the expression (4.8) and demanding that $\tilde{\rho} \to 0$ if $r \to \infty$ yields

$$\tilde{\rho}(r,z,t) = -\frac{F^2 z}{4\pi}\frac{1}{\left(2\Lambda^2+(4/Re)t\right)^2}\frac{1}{\left(1+(4/Re)t\right)^3}\exp\left(-\frac{2z^2}{2\Lambda^2+(4/Re)t}\right) \times \exp\left(-\frac{2r^2}{1+(4/Re)t}\right). \quad (4.13)$$

The maximum value of the density perturbation is then given by

$$\tilde{\rho}_{\max}(t) = \frac{F^2}{8\pi e^{1/2}(2\Lambda^2 + (4/Re)t)^{3/2}(1 + (4/Re)t)^3}. \tag{4.14}$$

For a convenient interpretation of the (non-dimensional) density perturbation $\tilde{\rho}$, the corresponding (dimensional) displacement Δz of the isopycnals can easily be derived. For a linear ambient density profile one can see that the (dimensional) density difference $\Delta\rho$ over a distance Δz is

$$\Delta\rho = \frac{\mathrm{d}\bar{\rho}}{\mathrm{d}z}\Delta z \tag{4.15}$$

and because $\tilde{\rho}$ has been non-dimensionalized by $N^2 L\rho_0/g = |\mathrm{d}\bar{\rho}/\mathrm{d}z|L$ the displacement of an isopycnal for a given value of $\tilde{\rho}$ is thus given by

$$\Delta z = \left|\frac{\mathrm{d}\bar{\rho}}{\mathrm{d}z}\right|^{-1}(N^2 L\rho_0/g)\tilde{\rho} = L\tilde{\rho}. \tag{4.16}$$

For example, a value $\tilde{\rho} = 0.01$ implies that an isopycnal has been displaced over a vertical distance equal to one percent of the length scale L. It can be seen from (4.13) that isopycnals are depressed ($\Delta z < 0$) in the upper part ($z > 0$) of the vortex and elevated ($\Delta z > 0$) in the lower part ($z < 0$) of the vortex, and this is in agreement with the density measurements in figure 6. It is important to note that in this diffusion model the time dependence of $\tilde{\rho}$ follows directly from the decay of v_θ. This is somewhat remarkable, since temporal changes of $\tilde{\rho}$ can only be caused by diffusion of salt (the stratifying agent) or by vertical transport of fluid elements, see equation (2.5). However, under the conditions used in the diffusion model (i.e. $v_z = 0$, $\partial/\partial\theta = 0$ and consequently $v_r = 0$) equations (2.3) and (2.5) are decoupled. Equation (2.3), in a reduced form given by the set (4.1)–(4.3), is therefore sufficient to describe an instantaneous relationship between the velocity field v_θ, the pressure $\tilde{p}$ and the density perturbation $\tilde{\rho}$.

Another remarkable result of the model is the fact that for certain combinations of F and Λ expression (4.13) represents an unstable density distribution. The criterion for the stability of a stratified fluid is given by $\partial\rho/\partial z \leqslant 0$, meaning that the density of the fluid should not decrease with increasing depth. In non-dimensional variables this criterion can be written as $\partial\tilde{\rho}/\partial z \leqslant 1$. In figure 7(*a*) the stability diagram for (4.13) is given in (F, Λ)-space. Two examples are shown in figure 7(*b*). For $\Lambda = 0.2$ and $F = 0.6$ the deformed density profile contains a region with a positive density gradient, whereas for $F = 0.3$ and the same Λ the density gradient is always negative. This implies that for certain combinations of F and Λ a balanced vortex might not be able to exist, according to the diffusion model.

To summarize, the complete diffusion model is given by the expressions for the azimuthal velocity $v_\theta(r, z, t)$, yielding the two vorticity components $\omega_r(r, z, t)$ and $\omega_z(r, z, t)$, and the density perturbation $\tilde{\rho}(r, z, t)$. Figure 8 shows the distributions of the vertical and radial vorticity components, of the vortex lines, and of the density perturbation in the (r, z)-plane for a typical monopolar vortex in a stratified fluid. Solid lines indicate positive values, dashed lines negative values. The vortex has a core of positive (vertical) vorticity, surrounded by a ring of negative (vertical) vorticity (figure 8*a*). The radial vorticity is positive in the upper part of the vortex and negative in the lower part (figure 8*b*). Contour plots of the quantity $\xi = rv_\theta$ are shown in figure 8(*c*). Since for an axisymmetric vortex (with $v_r = 0$ and $v_z = 0$) ξ-isolines are always tangent to the local vorticity vector, the ξ-contours indicate how the vortex lines form

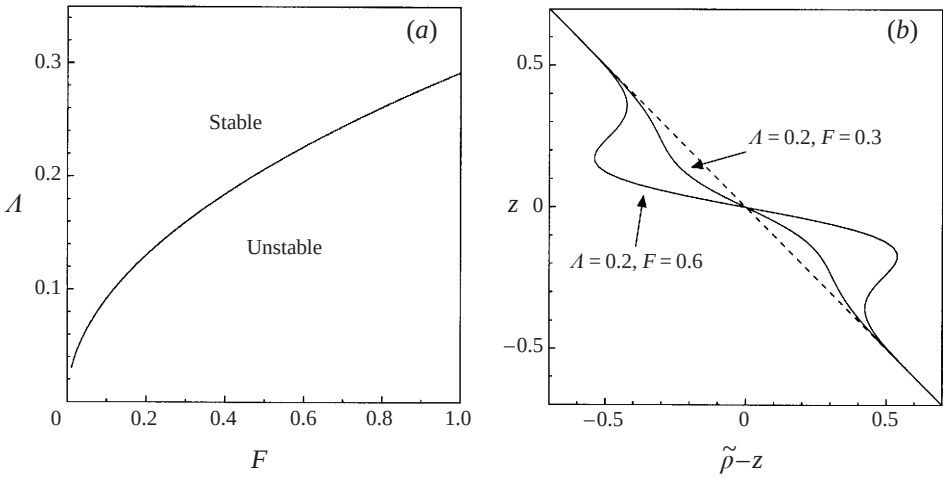

FIGURE 7. (*a*) Stability diagram that indicates for which values of F and Λ the initial density profile, (4.12) for $t = 0$, is (un)stable. (*b*) Examples of a stable ($F = 0.3$) and unstable ($F = 0.6$) density profile for a vortex with $\Lambda = 0.2$.

closed loops inside the fluid. Finally, figure 8(*d*) shows the distribution of the density perturbation. Above the vortex midplane isopycnals are deflected downwards ($\tilde{\rho} < 0$), while below this plane they are deflected upwards ($\tilde{\rho} > 0$).

5. Numerical simulations

In the previous section a simple, but useful, diffusion model has been derived, that describes how the strength of the vortex decreases in time due to diffusion of momentum and how the linear density distribution is perturbed by the presence of the vortex. The nature of the diffusion model (no radial and vertical motions are allowed) has resulted in the rather remarkable fact that the density perturbation is supposed to adjust instantaneously to the velocity distribution. To gain a more detailed insight in the dynamics of a vortex in a stratified fluid, additional numerical simulations are performed that solve the complete set of governing equations (2.3)–(2.5). These simulations might reveal to what extent the results of the diffusion model are compatible with the real flow dynamics and allow a study of the influence of the governing parameters of the flow in a systematic way. Comparison between the results of the laboratory experiments, the diffusion model and the simulations can then give a complete survey of the dynamics of axisymmetric vortices in a stratified fluid.

5.1. *Initial conditions*

In a first set of simulations, the role of the cyclostrophic balance in the dynamics of the vortex is investigated by using different initial conditions. More particularly, by using the velocity and density fields derived from the diffusion model three initial situations are considered. In case 1 the response of the stratified fluid to an initial perturbation of the density $\tilde{\rho}(r, z)$, i.e. (4.13) for $t = 0$, without imposing any velocity field, is investigated. The initial density distribution is sketched for two isopycnals in figure 9(*a*). It is to be expected that in case 1 the buoyancy force $\boldsymbol{F}_{\mathrm{buo}} = -(1/F^2)\tilde{\rho}\boldsymbol{e}_z$, see equation (2.3), will immediately bring the disturbed isopycnals back to their original positions (dashed lines). This process is illustrated in figure 9(*b*). Due to the

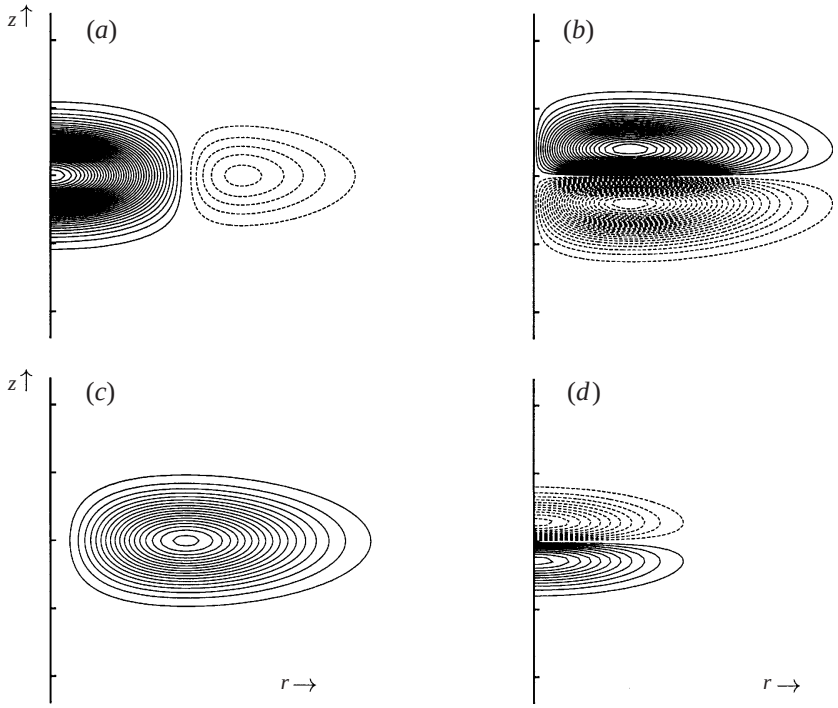

FIGURE 8. Spatial distribution of the vorticity and density perturbation in the (r,z)-plane for the vortex described by the model, see equation (4.8). (*a*) $\omega_z(r,z)$, (*b*) $\omega_r(r,z)$, (*c*) $\xi(r,z)$, (*d*) $\tilde{\rho}(r,z)$. The increments in the values represented by the contours are $\Delta\omega = 0.05$, $\Delta\xi = 0.02$, $\Delta\tilde{\rho} = 0.005$ (with $A = 0.2$ and $F = 0.23$). Continuous contours represent positive values, dashed contours represent negative values.

conservation of mass, the restoration of the isopycnals will induce a radially inward flow, and it is likely that a temporary circulation pattern will be formed as indicated by the arrows. In case 2 the initial flow is given by the velocity distribution $v_\theta(r,z)$, i.e. (4.8) for $t = 0$, but no perturbation of the density distribution is prescribed. This situation is sketched in figure 9(*c*). Initially the isopycnals (ρ_1 and ρ_2) are horizontal (continuous lines), but due to the centrifugal force $\boldsymbol{F}_c$, caused by the velocity field, fluid is accelerated radially outwards. This generates a circulation pattern as illustrated by the arrows, and consequently, the isopycnals will become deformed (dashed lines). This process is called the cyclostrophic adjustment of the vortex. Finally, in case 3 both the velocity distribution $v_\theta(r,z)$ and the associated density perturbation $\tilde{\rho}(r,z)$ are prescribed, so that the initial vortex is in cyclostrophic balance. This simulation can then illustrate whether the balance is maintained during the decay of the vortex.

5.1.1. *The response of a stratified fluid to an initial density perturbation* (*case* 1)

In a stably stratified fluid all isopycnals, i.e. planes of constant density, are horizontal, but when such an isopycnal is locally elevated or depressed the buoyancy force will restore the balance by forcing the isopycnal back to its original level. The response of the stratified fluid to the initial density perturbation is shown in figure 10. Contour plots of the azimuthal vorticity ω_θ and of the density perturbation $\tilde{\rho}$ in the (r,z)-plane are shown in (*a*) and (*b*), respectively. The azimuthal vorticity component,

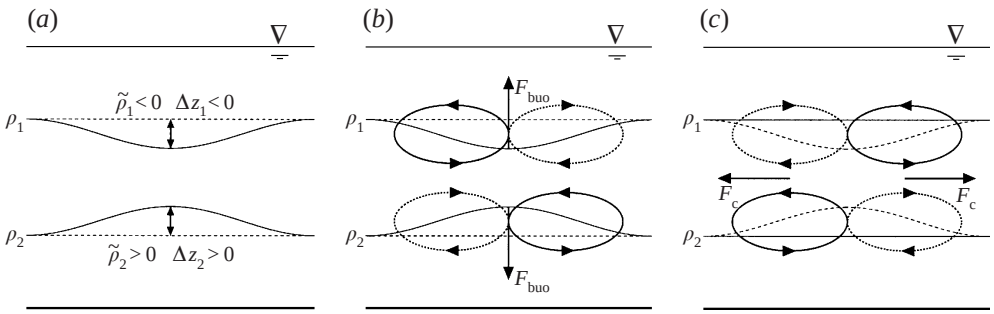

FIGURE 9. (*a*) Sketch of the shape of two isopycnals (ρ_1 for $z > 0$, ρ_2 for $z < 0$) for the density perturbation given by (4.12). (*b*) Schematic drawing of the circulation pattern induced by the buoyancy force $\boldsymbol{F}_{\mathrm{buo}}$ due to the release of a density perturbation as in (*a*). (*c*) Schematic drawing of the circulation pattern due to the centrifugal force $\boldsymbol{F}_{\mathrm{c}}$ in a vortex that is (initially) not in cyclostrophic balance.

defined by

$$\omega_\theta = \frac{\partial v_r}{\partial z} - \frac{\partial v_z}{\partial r}, \tag{5.1}$$

gives an impression of the flow field in the (r, z)-plane. Positive ω_θ can thus be associated with clockwise shearing motions, and *vice versa*. The contours of ω_θ in figure 10(*a*) illustrate that immediately after the initialization of the flow, a circulation pattern is indeed generated, as was sketched in figure 9(*b*) and isopycnals move back to their undisturbed positions, as indicated by the strong decrease of $\tilde{\rho}$ in figure 10(*b*). During the adjustment process the isopycnals overshoot their equilibrium positions, and this results in the generation of internal waves, clearly illustrated by the elongated, inclined ω_θ- and $\tilde{\rho}$-patches at $t = 2$. Similar adjustment processes to localized perturbations of the density distribution of a stratified fluid have been reported by Wu (1969), Hartman & Lewis (1972) and Terez & Knio (1998). These papers describe the response of a stratified fluid to the presence of a region with partially mixed or homogeneous fluid. In fact such a region can be represented by a perturbation as in figure 9(*a*), but with the isopycnals deflected in the opposite direction. Also, these adjustment processes result in the generation of internal waves.

The generation of azimuthal vorticity ω_θ can also be recognized as the baroclinic production of vorticity, see Lighthill (1978, 1996). This theorem can be explained by using the vorticity equation, which can be obtained by taking the curl of equation (2.3). It states that when vertical displacements of fluid parcels in a stably stratified fluid lead to horizontal gradients in the density this results in the production of vorticity in a direction perpendicular to the plane formed by gravity $\boldsymbol{g}$ and $\nabla\rho$. For an axisymmetric density perturbation this thus leads to the production of vorticity in the azimuthal direction.

5.1.2. *The initially unbalanced vortex* (*case* 2)

The diffusion model has shown that cyclostrophic balance of a vortex in a linearly stratified fluid is only possible when the isopycnals are deformed inside the vortex. This conclusion can be investigated by studying the response of the stratified fluid to the velocity distribution of a vortex, but without the accompanying density perturbation. Figure 11 shows contour plots of the azimuthal vorticity and of the density perturbation in the (r, z)-plane at four times. As illustrated in figure 9(*c*), the centrifugal force inside the vortex does indeed cause a (secondary) circulation in the

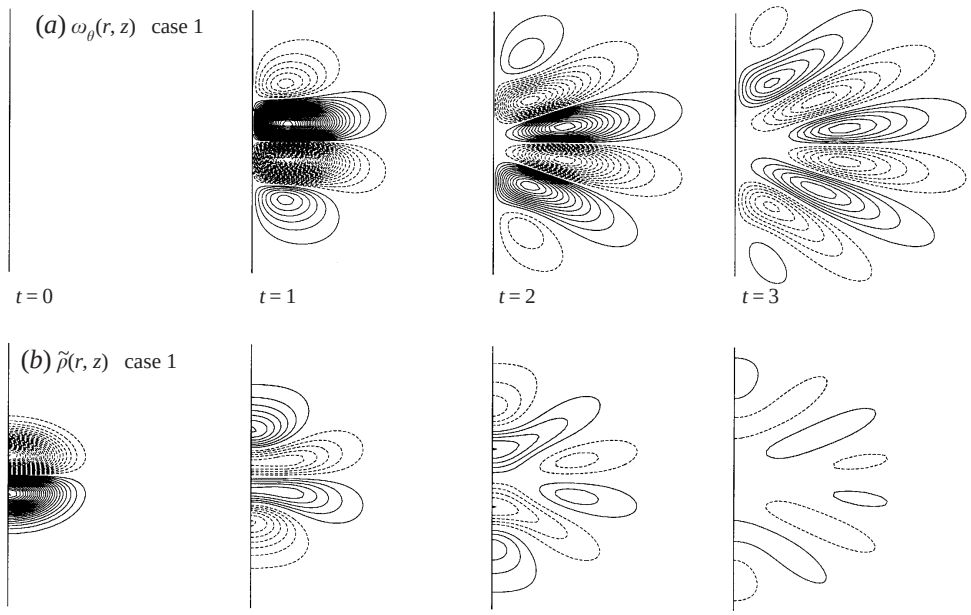

FIGURE 10. Contour plots in the (r, z)–plane of the azimuthal vorticity $\omega_\theta(r, z)$ in (a), and of the density perturbation $\tilde{\rho}(r, z)$ in (b) for $t = 0$, 1, 2 and 3, for the numerical simulation case 1. The increments in the contour values are $\Delta\tilde{\rho} = 0.0005$ and $\Delta\omega_\theta = 0.002$ and the parameters of the simulation are $A = 0.4$, $Re = 100$, $F = 0.3$ and $Sc = 10$.

(r, z)-plane. In figure 11(a) one observes, immediately after the initialization, an azimuthal vorticity distribution that can be associated with counterclockwise circulation in the region $z > 0$ and clockwise circulation for $z < 0$. At the same time isopycnals above and below the vortex are deflected towards the vortex symmetry plane $z = 0$: $\tilde{\rho} < 0$ for $z > 0$ and $\tilde{\rho} > 0$ for $z < 0$. In other words, the circulation in the (r, z)-plane generates the density perturbation that provides the necessary pressure gradient force to balance the centrifugal force. The vortex is then in cyclostrophic balance. Just as in the previous case, the sudden adjustment of the flow results in the generation of internal waves that are radiated away from the centre of the vortex.

5.1.3. *The initially balanced vortex* (*case* 3)

One might expect that a vortex that is initially in cyclostrophic balance will show none (or perhaps only very little) adjustment, because the centrifugal force is already balanced. Figure 12 presents the results of a simulation for such an initially balanced vortex. However, one can still observe a weak secondary circulation and small changes in the shape of the density perturbation. The reason for this behaviour is the decay of the vortex due to diffusion. The strength of the vortex decreases in time, so the flow only remains in balance when the radial pressure gradient (due to the perturbation of the isopycnals) also decreases. The diffusion of salt (the density stratifying agent) cannot account for such a fast decay of the density perturbation, because salt diffuses on a much larger time scale than momentum. Consequently, a buoyancy-driven flow will arise, similar to the one illustrated in figure 9(b), until the centrifugal force and the pressure gradient force inside the vortex are again in balance. Such a suggested circulation pattern can indeed be observed in the azimuthal vorticity distribution in figure 12(a): there is a clockwise circulation in the upper part and a counterclockwise

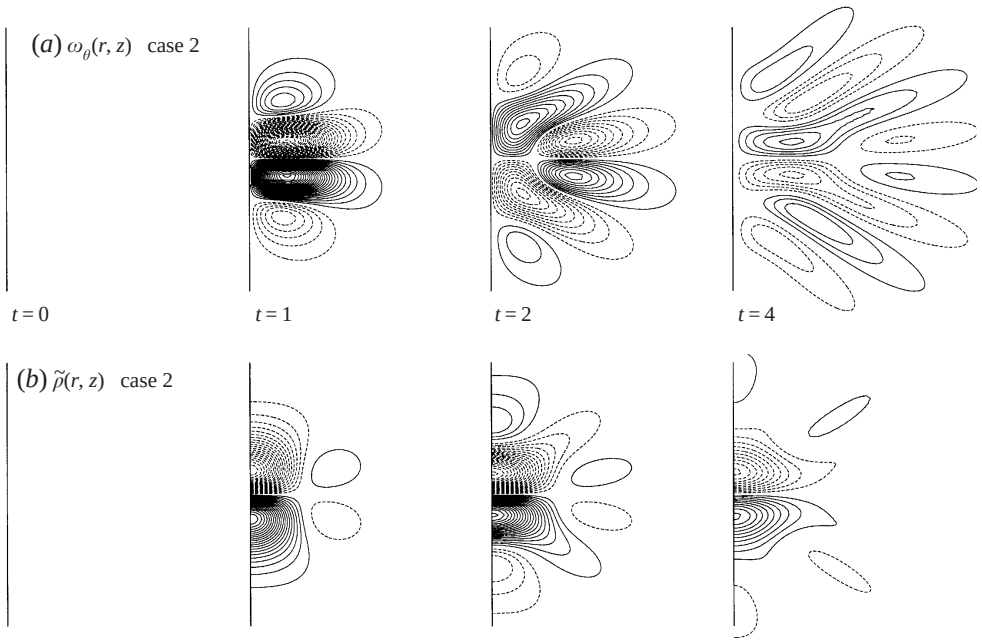

FIGURE 11. Similar to figure 10, but now for the numerical simulation case 2.

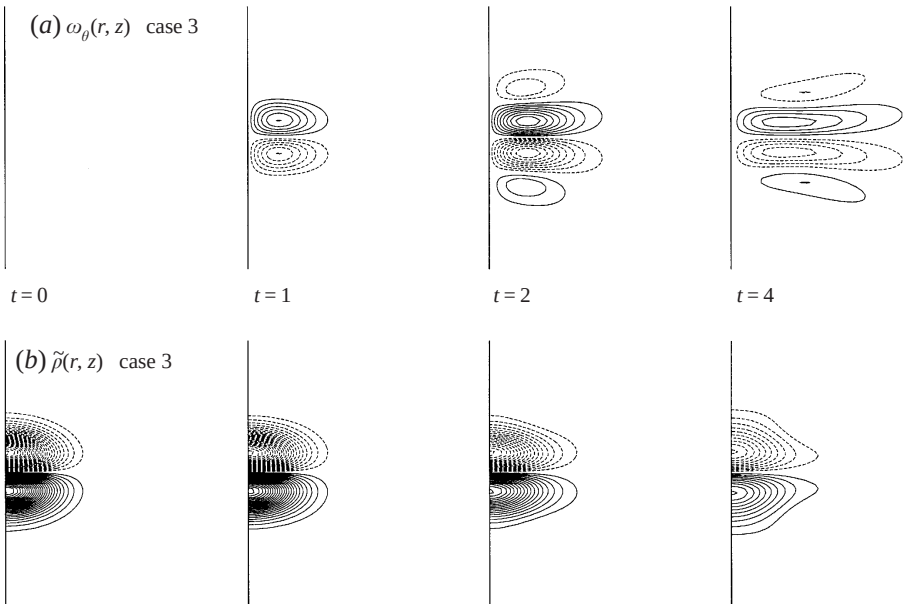

FIGURE 12. Similar to figure 10, but now for the numerical simulation case 3.

circulation in the lower part of the vortex. As the azimuthal vorticity is absent in the diffusion model (because $v_r = 0$ and $v_z = 0$) the maximum value of ω_θ can thus be regarded as a convenient measure to express the deviation of the vortex from the Q2D diffusion model during its decay.

5.2. *The influences of Sc, F and Re*

The Schmidt number, defined by $Sc = \nu/\kappa$, gives the ratio between the diffusivities of momentum and salt. For a vortex in a stratified environment this ratio has an important influence on the flow dynamics. In the previous simulations a Schmidt number of $Sc = 10$ has been used, but in fact for the diffusivity of salt in water† the Schmidt number is much larger: $Sc \approx 700$.

To investigate the effect of the Schmidt number in more detail similations similar to case 3 are performed, but now for $Sc = 1$, 10, 50 and 100. For the (imaginary) case of $Sc = 1$ one might expect that the initial density perturbation decays exactly as fast as the velocity distribution. This suggests that the vortex can stay in cyclostrophic balance during its decay, without generating a secondary circulation pattern and consequently its decay may be described by the diffusion model. Figure 13 shows the results of the comparison between the evolution of the maximum values of the density perturbation $\tilde{\rho}_{\max}$ and of the azimuthal vorticity $\omega_{\theta\max}$ for different Sc. For $Sc = 1$ the decay of the density perturbation agrees very well with the diffusion model, represented by the line $\tilde{\rho}_{\max}(t)$. The vortex is thus very close to cyclostrophic balance during its decay. For higher values of Sc this appears not to be the case, because initially the decay of the density perturbation is slower than in the diffusion model. The production of azimuthal vorticity (see figure 13*b*), which can be regarded as an indicator of to what extent the flow deviates from the flow predicted by the diffusion model, shows that for $Sc = 1$ the secondary circulation is very small. However, it is not exactly zero, since the diffusion of momentum and density (salt) are not governed by exactly the same equations:

$$\frac{\partial v_\theta}{\partial t} + (\boldsymbol{v}\cdot\nabla)v_\theta + \frac{v_r v_\theta}{r} = \frac{1}{Re}\left(\nabla^2 v_\theta - \frac{v_\theta}{r^2}\right) \tag{5.2}$$

and

$$\frac{\partial \tilde{\rho}}{\partial t} + (\boldsymbol{v}\cdot\nabla)\tilde{\rho} - v_z = \frac{1}{Sc\ Re}\nabla^2\tilde{\rho}. \tag{5.3}$$

Even when initially $v_r = 0$, $v_z = 0$ and $Sc = 1$, v_θ and $\tilde{\rho}$ will evolve differently, due to the difference between their diffusion terms. This then results in an inbalance in the vortex and the generation of a small secondary circulation (i.e. v_r and v_z are no longer zero).

It may seem remarkable that for $Sc = 10, 50$ and 100 there is little difference between the evolution of $\tilde{\rho}_{\max}$ and $\omega_{\theta\max}$. This is, however, due to the fact that for $Sc = 10$ the characteristic time scale for the diffusion of salt can be regarded as already very large compared to the decay time scale of the vortex. Even larger values of Sc do not alter these results substantially.‡ In general it is difficult to perform well resolved simulations for realistic values of the Schmidt number, i.e. $Sc \approx 700$,

† Note that for a thermally (instead of salt) stratified fluid a similar mechanism will take place, but here the ratio between the diffusivities is called the Prandtl number. For thermally stratified water the Prandtl number has a value of $Pr \approx 7$ (at 20 °C). For thermally stratified air the Prandtl number is even smaller than 1: $Pr \approx 0.7$ (at 20 °C). This latter case is particularly interesting, because for $Pr < 1$ momentum diffuses slower than the stratifying agent. As a result this type of flow is governed by a entirely reversed dynamics. However, this case is beyond the scope of the present paper.

‡ Convergence tests were performed for the case of $Sc = 100$ (for grids up to 512×512 gridpoints) and no significant differences could be observed. The reason for this is that when the Schmidt number is large, gradients of $\tilde{\rho}$ decrease much faster by the redistribution of $\tilde{\rho}$ due to the secondary circulation pattern, than due to diffusion.

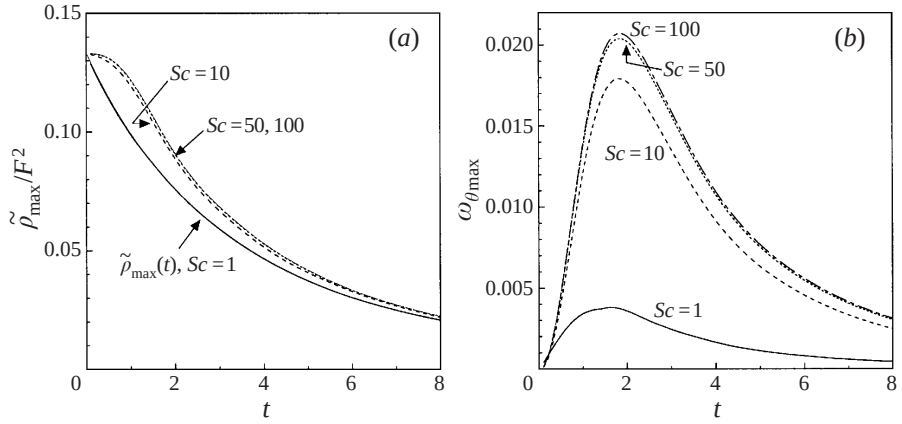

FIGURE 13. Evolution of the maximum values of the density perturbation $\tilde{\rho}_{\max}$ and of the azimuthal vorticity $\omega_{\theta\max}$ for a decaying vortex with an initial density perturbation, i.e. similar to case 3. The results are shown for four simulations with different Schmidt numbers (with $Re = 100$, $F = 0.3$ and $A = 0.4$).

particularly for higher Reynolds numbers. Fortunately, however, the results shown in figure 13 indicate that this is not necessary. It is reasonable to perform numerical simulations of axisymmetric vortices in a linearly stratified fluid with $Sc = 10$, without dramatically changing the flow dynamics compared to real experimental conditions ($Sc \approx 700$).

The Froude number represents the relative strength of the inertial force and the buoyancy force in the flow. It was shown in (4.16) that the deflection of the isopycnals inside a vortex is directly proportional to the density perturbation, $\Delta z = L\tilde{\rho}$, and expression (4.13) indicates that the density perturbation is proportional to F^2. In other words, the smaller the Froude number is, the smaller is the deflection of the isopycnals and the weaker the secondary circulation during the decay of the vortex will be. It is therefore obvious that fluid motion inside a vortex in a linearly stratified fluid can be better approximated by strictly two-dimensional flow when F becomes smaller. This is illustrated in figure 14, where for three different cases ($F = 1.0$, $F = 0.3$ and $F = 0.1$) the maximum values of $\tilde{\rho}$ and ω_θ are plotted as a function of time. The comparison with the diffusion model clearly shows that for the lowest Froude number the differences between the simulated flow and the diffusion model ($\tilde{\rho}_{\max}(t)$) are almost negligible and, furthermore, that the production of ω_θ tends to vanish as F decreases.

Further numerical simulations are performed to investigate the effect of the Reynolds number. In particular the same case as that of figure 12 is simulated for $Re = 500$ and $Re = 1000$. However, the results, except for a slower decay of $\tilde{\rho}$ and ω_z, do not show striking differences. Besides, when the time is scaled with the factor $4/Re$ the results for different Reynolds numbers all collapse onto one single curve. This is due to the fact that the Reynolds number changes the diffusion time scale of both the momentum and the density by the same amount. However, it is observed in some of the experiments as well as in a few preliminary three-dimensional simulations that the Reynolds number plays an important role in the stability of the vortex with respect to azimuthal perturbations. This topic, however, is beyond the scope of the present paper and will be the subject of a forthcoming study.

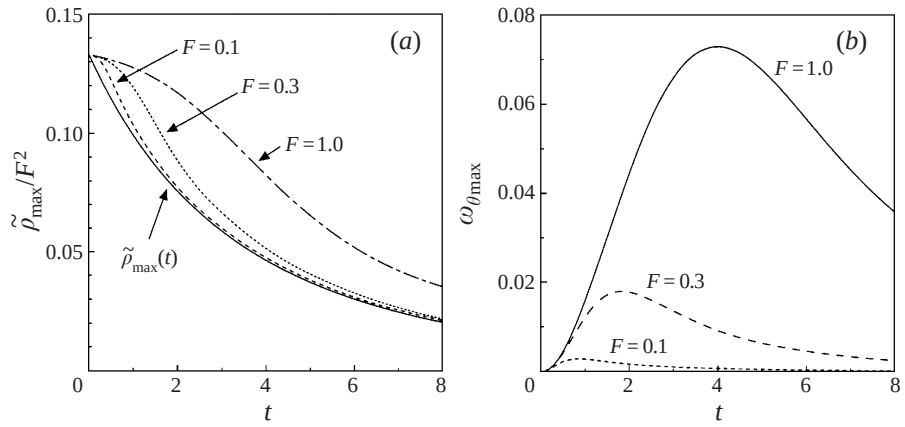

FIGURE 14. As in figure 13, but now for three simulations for three different Froude numbers (with $Re = 100$, $Sc = 10$ and $\Lambda = 0.4$).

5.3. *Vortex stretching*

We found that the secondary circulation during the decay of a vortex decreases for smaller Froude number flows and it was concluded that the vortex agrees better with the diffusion model. However, the influence of the secondary circulation on the vortex itself has not yet been addressed. A possible effect of the secondary circulation is illustrated in figure 15. During the decay of the vortex the isopycnals move back to their undisturbed positions and a radially inward flow takes place inside the vortex. This process is called *vortex stretching*, during which potential energy that is stored in the perturbation of the isopycnals is converted into kinetic energy of the vortex. Combined with the effects of vertical and radial diffusion of momentum the stretching process will lead to a reduced decay rate of the vorticity at the symmetry plane and a reduced radial growth of the vortex. Figure 16(a, b) shows the evolution of the maximum values of ω_z (i.e. in the core of the vortex at the symmetry plane $z = 0$) and of the vortex radius $\hat{r}$ (i.e. the radius at $z = 0$ where the vertical vorticity changes sign) for three different Froude number flows, while keeping the initial vortex thickness fixed ($\Lambda = 0.3$). The dashed lines represent results from the diffusion model for similar initial conditions, given by (4.11) and (4.9). It is observed that for $F = 0.1$ both the decay of the vortex and its radial growth are described well by the diffusion model. However, for larger values of F, especially $F = 1.0$, the vortex decays at a much slower rate than according to the diffusion model. At the same time the vortex temporarily ceases to grow in the radial direction. A similar behaviour is observed in figure 16(c, d) where the results are compared between simulations for two vortices with different initial thicknesses ($\Lambda = 0.2$ and 0.4), while keeping the Froude number fixed ($F = 0.3$). For $\Lambda = 0.4$ the decay and growth of the vortex are both characterized well by the diffusion model, whereas for the thinner vortex the decay rate becomes smaller and the radial growth holds for a moment.

The results in figure 16 illustrate that for small Froude number flows the diffusion model gives a good representation of the decay of the vortex. It is not our objective here to include the stretching effects in a more elaborate model, because it will be shown later that for the present laboratory experiments the stretching effects are of limited importance. Besides, the deviations from the model for a large Froude number and a small initial vortex thickness can be explained by the following example.

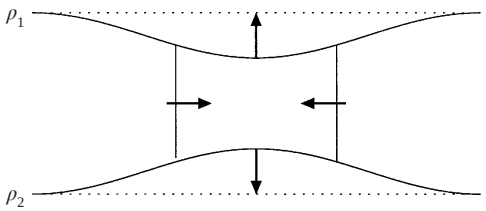

FIGURE 15. Illustration of the deformation of two isopycnals in a vortex. During the decay of the vortex the isopycnals relax to their undisturbed positions and the vortex is stretched.

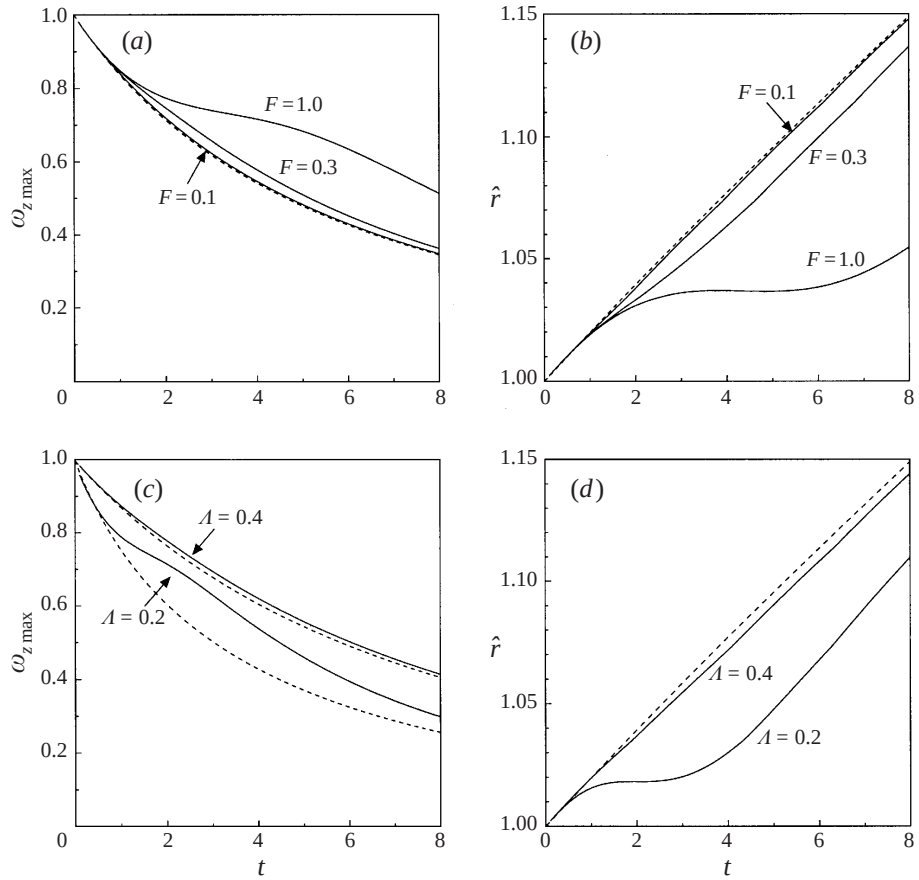

FIGURE 16. (*a*) Evolution of the maximum values of ω_z (normalized by their initial values) for three cases with different values of F (with $Re = 100$, $\Lambda = 0.3$ and $Sc = 10$. (*b*) The corresponding evolution of the radius of the vortex cores, $\hat{r}$. (*c*) Similar to (*a*), but now for two vortices with different initial thickness Λ (with $Re = 100$, $F = 0.3$ and $Sc = 10$). (*d*) Similar to (*b*). The dashed lines represent the decay and growth of the vortices according to the diffusion model, (4.11) and (4.9) respectively.

Suppose that the vortex is represented by a cylinder of fluid with thickness H_0, which is in solid body rotation with angular velocity Ω_0, between two isopycnals. During the decay of the vortex the thickness of the vortex will increase by an amount ΔH, due to the relaxation of the isopycnals. Simultaneous conservation of mass and conservation

of angular momentum then yields an expression for the relative change in Ω for a given relative change in H:

$$\frac{\Delta\Omega}{\Omega_0} = \frac{\Delta H}{H_0}. \tag{5.4}$$

Equations (4.14) and (4.16) show that $\Delta H \sim \tilde{\rho}$ and $\tilde{\rho}_{\max} \sim F^2/\Lambda^3$, so that $\Delta\Omega/\Omega_0 \sim F^2/\Lambda^4$. In other words, the stretching process in a vortex with a small value of Λ or for a large Froude number leads to a much more profound change in the vorticity than for a vortex with a larger value for Λ or a smaller Froude number. For example, this implies that the effect of the vortex stretching is approximately 16 times stronger for the vortex with $\Lambda = 0.2$ compared with $\Lambda = 0.4$. Similarly the stretching effect becomes approximately 10 times stronger for the case with $F = 1.0$, compared to $F = 0.3$. These estimates appear to correspond quite well to the results in figures 16(*a*) and 16(*c*).

5.4. *Comparisons between experiments, model and simulations*

In order to make a comparison of the experimental results with the diffusion model and with numerical simulations, it is necessary to calculate values for $Re = VL/\nu$ and $F = V/(LN)$. These numbers include the length scale L, the velocity scale V and the buoyancy frequency N. The last is obtained by measurement of the density profile, as described in § 2.1, yielding $N = 1.9\,\mathrm{rad\,s^{-1}}$. The length scale L was found to be defined by the initial radial position in the vortex, where the vorticity changes sign and it can be estimated from the cross-section as in figure 3. This yields $L \approx 3\,\mathrm{cm}$, although this value is only an estimate because the vortex is not always entirely axisymmetric. Furthermore, information about the vertical extent of the vortex is obtained by estimating $\Lambda = \lambda/L$. From the experimental results it appears that $\Lambda \approx 0.3$. As illustrated before, the velocity scale V can be estimated by $V = (2\pi)^{1/2}\lambda\omega_M$, with ω_M the experimentally observed initial maximum value of the vorticity.

The choice of the time at which the above parameters are evaluated is an important issue. In § 2.1 we have mentioned that the time origin ($t = 0$) was defined as the moment the injection of fluid was stopped. At that moment, however, the vortex is not well-defined, because the injection cylinder is still present in the fluid. It is therefore more reliable to choose a later time to define parameters for *the initial vortex*, and in the present experiment we use $t_0 = 40\,\mathrm{s}$, yielding $V = 1.7\,\mathrm{cm\,s^{-1}}$. Another choice of t_0 will in general lead to other values for Re and F, because these numbers define the 'initial condition' of the vortex at another moment. The present parameters are $Re = 500$, $F = 0.3$ and $\Lambda = 0.3$. To compare the experimental results with the diffusion model, time and vorticity are non-dimensionalized by the transformations $t' = (t - t_0)V/L$ and $\omega'_{z\,\max} = \omega_{z\,\max}L/V$ and the primes are omitted. The evolution of the maximum vorticity in the vortex at $z = 0$ and $z = 2$ cm are compared with the model, given by (4.11), and with a numerical simulation, initialized by the same parameters, in figure 17(*a*). Especially for $z = 0$ there appears to be a good correspondence between the experimentally observed decay and the diffusion model. The deviation of the results with the diffusion model for $z = 2$ cm is most likely caused by the inaccuracies in z and Λ. The lightsheet has a thickness of approximately 0.5 cm and the tracer particles have a natural spreading in their vertical distribution. Another deviation of the measurements from the model is the slightly higher vorticity at late times in the experiments. This is likely to be caused by a weak (solid body) background rotation in the tank, which only becomes noticeable when the vortex rotates very slowly. The very close agreement between the results of the numerical

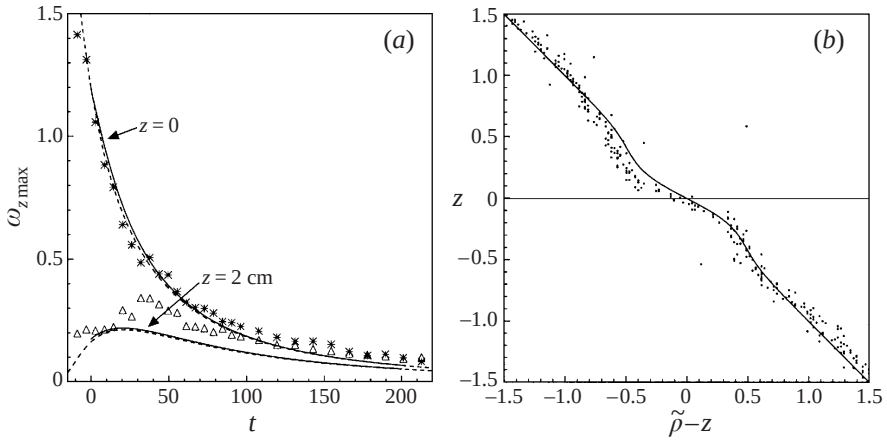

FIGURE 17. (*a*) Comparison between the experimentally obtained vorticity decay shown in figure 4 (symbols), the diffusion model (4.11), represented by the dashed lines and numerical simulations (thick continuous lines) showing decay of a vortex under experiment conditions: $Re = 500$, $\Lambda = 0.3$, $F = 0.3$ and $Sc = 10$. (*b*) Comparison between the measured density profile shown in figure 6 (*c*) (represented in a non-dimensional form ($\tilde{\rho} - z$) as a function of the non-dimensional height z) and the density distribution according to the model, given by expression (4.13) for $r = 0$ and calculated for the case of $F = 0.7$ and $\Lambda = 0.3$.

simulation and the diffusion model shows that for the present flow conditions, the effects of stretching during the decay of the vortex are almost negligible.

We can also make an estimate of the perturbation of the density profile for a vortex under laboratory conditions, which can be compared to the experiment shown in figure 6(*c*). For $t = 22\,\mathrm{s}$ the value for V is estimated by using the value for the maximum vorticity at $t = 20\,\mathrm{s}$ in figure 5(*a*), which yields $V = 2.3\,\mathrm{cm\,s^{-1}}$. With $L = 3\,\mathrm{cm}$ and $N = 1.0\,\mathrm{rad\,s^{-1}}$ we find that $F = 0.7$ and furthermore we assume that $\Lambda = 0.3$. Using these values the density profile is computed from (4.13) for $r = 0$, and the results are presented in figure 17(*b*). Considering the fact that the calculated density distribution represents only an estimate, it should be considered as an order of magnitude approximation, which still agrees quite well with the experimentally measured density perturbation. The maximum density perturbation is $\tilde{\rho}_{\max} \approx 0.2$, and we can estimate the maximum deflection of the isopycnals in this experiment: $\Delta z_{\max} = L\tilde{\rho}_{\max} \approx 0.6\,\mathrm{cm}$.

6. Conclusions

The comparison of the results of laboratory experiments with an analytical model and with numerical simulations has led to a better insight into the dynamics of an axisymmetric vortex in a linearly stratified fluid. The distribution of the vertical component of the vorticity in different horizontal planes inside the vortex has been measured, as well as the vertical density profile through the centre of the vortex. The diffusion model, which has been derived from the Boussinesq equations under the assumption of a purely axisymmetric swirling flow, has provided analytical expressions for the three-dimensional time-dependent distributions of velocity and density inside the vortex.

The laboratory experiments confirmed that inside the vortex the density profile is deformed: above and below the vortex isopycnals are deflected towards the symmetry

plane. The numerical simulations performed for a vortex in a linearly stratified fluid under various initial conditions revealed that in the absence of an initial density perturbation the centrifugal force inside the vortex induces a circulation that results in the deformation of the isopycnals. The vortex is then in cyclostrophic balance.

Furthermore, numerical simulations have shown that when the time scales of diffusion of momentum (vorticity) and of the stratifying agent (salt) are disparate, i.e. when $Sc \gg 1$, the decay of the vortex is accompanied by a buoyancy-induced secondary circulation. This circulation results from the fact that the cyclostrophic balance in the vortex is disturbed during the decay and it causes a redistribution of the density inside the vortex. The vortex therefore becomes stretched during its decay. In other words, potential energy stored in the density perturbation is converted into kinetic energy of the vortex, so that the decay of the vortex starts to deviate from the decay described by the diffusion model. However, it has been shown that for flow conditions that apply to the laboratory experiments the stretching effect is almost negligible and the decay of the vortex is described well by the diffusion model.

One of the authors (M. B.) gratefully acknowledges financial support by the Dutch Foundation for Fundamental Research on Matter (FOM). Additional financial support from the J. M. Burgers Centre for a working visit of R. V. to Eindhoven is also gratefully appreciated. The authors thank Martijn de Bruijn for his contribution to the laboratory experiments.

Appendix. The solution of the diffusion equation

The diffusion equation (4.2) is solved by the method of separation of variables. Suppose that

$$\hat{v}_\theta(r,z,t;k,l) = \hat{G}(r;k)\hat{H}(z;l)\hat{T}(t;k,l) \tag{A 1}$$

is a solution of the diffusion equation. Substitution of this expression in (4.2) and dividing by $\hat{G}(r)\hat{H}(z)\hat{T}(t)$ results in

$$Re\frac{1}{\hat{T}}\frac{\mathrm{d}\hat{T}}{\mathrm{d}t} = \frac{1}{\hat{G}}\frac{\mathrm{d}^2\hat{G}}{\mathrm{d}r^2} + \frac{1}{r\hat{G}}\frac{\mathrm{d}\hat{G}}{\mathrm{d}r} - \frac{1}{r^2} + \frac{1}{\hat{H}}\frac{\mathrm{d}^2\hat{H}}{\mathrm{d}z^2}. \tag{A 2}$$

Separation of variables for this equation yields three separate differential equations for $\hat{G}$, $\hat{H}$ and $\hat{T}$:

$$\frac{\mathrm{d}^2\hat{G}}{\mathrm{d}r^2} + \frac{1}{r}\frac{\mathrm{d}\hat{G}}{\mathrm{d}r} - \frac{\hat{G}}{r^2} = -k^2\hat{G}, \quad \frac{\mathrm{d}^2\hat{H}}{\mathrm{d}z^2} = -l^2\hat{H} \quad \text{and} \quad \frac{\mathrm{d}\hat{T}}{\mathrm{d}t} = -\frac{(k^2+l^2)}{Re}\hat{T}. \tag{A 3}$$

Solutions for these standard differential equations are

$$\hat{G}(r;k) = A(k)\,J_1(kr) + B(k)\,Y_1(kr), \tag{A 4}$$

$$\hat{H}(z;l) = C(l)\cos(lz) + D(l)\sin(lz), \tag{A 5}$$

$$\hat{T}(t;k,l) = \exp\left\{-\frac{1}{Re}(k^2+l^2)t\right\}, \tag{A 6}$$

where A, B, C and D are constants (i.e. independent of r, z and t), to be determined by boundary and initial conditions.

Boundary conditions are given by the constraint that the solutions should be finite for $r = 0$ and should vanish for $r \to \infty$. This results in $B = 0$. Additionally, by supposing that the fluid motion is initially even around $z = 0$, one finds that $D = 0$.

As there are no limitations on the domain in the r- and z-directions, k and l are not restricted to certain values. It is therefore possible to construct a general solution $v_\theta(r,z,t)$, which is given by

$$v_\theta(r,z,t) = \int_0^\infty \int_0^\infty A(k)\,J_1(kr)\,C(l)\,\cos(lz)\,\exp\left\{-\frac{1}{Re}(k^2+l^2)t\right\}\mathrm{d}k\,\mathrm{d}l. \qquad (A\,7)$$

The functions $A(k)$ and $C(l)$ are determined by using the initial condition for v_θ,

$$v_\theta(r,z,0) = \int_0^\infty A(k)\,J_1(kr)\,\mathrm{d}k \int_0^\infty C(l)\,\cos(lz)\,\mathrm{d}l \equiv G(r)\,H(z). \qquad (A\,8)$$

To determine the function $A(k)$ from the initial condition $G(r)$, the Hankel integral formula (see, e.g. Oberhettinger 1972) can be used. The radial part of the initial velocity distribution $v_\theta(r,z,0)$ can thus be written as

$$G(r) = \int_0^\infty A(k)\,J_1(kr)\,\mathrm{d}k = \int_0^\infty \left[k\int_0^\infty G(u)\,J_1(ku)u\,\mathrm{d}u\right] J_1(kr)\,\mathrm{d}k. \qquad (A\,9)$$

Hankel integrals are tabulated for various functions in Oberhettinger (1972). The function $C(l)$ can be computed by applying cosine transform techniques. Using the expressions (4.6) and (4.7) for $G(r)$ and $H(z)$ then yields

$$v_\theta(r,z,t) = \int_0^\infty \left[\int_0^\infty \frac{1}{8}k^2 \exp\left\{-\frac{1}{4}\left(\frac{4t}{Re}+1\right)k^2\right\} J_1(kr)\,\mathrm{d}k\right] \times \frac{1}{\pi}\exp\left\{-\left(\frac{t}{Re}+\frac{1}{2}A^2\right)l^2\right\}\cos(lz)\,\mathrm{d}l, \qquad (A\,10)$$

which can be written in an analytical form given by (4.8). The corresponding radial and vertical vorticity components are now given by

$$\omega_r = -\frac{\partial v_\theta}{\partial z} = \frac{rz}{\pi^{1/2}(2A^2+(4/Re)t)^{3/2}(1+(4/Re)t)^2} \times \exp\left(-\frac{z^2}{2A^2+(4/Re)t}\right)\exp\left(-\frac{r^2}{1+(4/Re)t}\right) \qquad (A\,11)$$

and

$$\omega_z = \frac{1}{r}\frac{\partial(rv_\theta)}{\partial r} = \frac{1}{\pi^{1/2}(2A^2+(4/Re)t)^{1/2}(1+(4/Re)t)^2}\left(1-\frac{r^2}{1+(4/Re)t}\right) \times \exp\left(-\frac{z^2}{2A^2+(4/Re)t}\right)\exp\left(-\frac{r^2}{1+(4/Re)t}\right). \qquad (A\,12)$$

REFERENCES

Beckers, M., Verzicco, R., Clercx, H. J. H. & Heijst, G. J. F. van 1999 Numerical study of the evolution of vortices in a linearly stratified fluid. *Il Nuovo Cimento* **22**, 847–856.

Bonnier, M., Eiff, O. & Bonneton, P. 1999 On the density structure of far-wake vortices in a stratified fluid. Submitted to *Dyn. Atmos. Oceans.*

Bower, A. S., Armi, L. & Ambar, I. 1997 Lagrangian observations of Meddy formation during a Mediterranean undercurrent seeding experiment. *J. Phys. Oceanogr.* **27**, 2545–2575.

Carton, X. J., Flierl, G. R. & Polvani, L. M. 1989 The generation of tripoles from unstable axisymmetric isolated vortex structures. *Europhys. Lett.* **9**, 339–344.

Chomaz, J. M., Bonneton, P., Butet, A. & Hopfinger, E. J. 1993 Vertical diffusion of the far wake of a sphere moving in a stratified fluid. *Phys. Fluids* A **5**, 2799–2806.

Dalziel, S. 1992 *DigImage. Image Processing for Fluid Dynamics.* Cambridge Environmental Research Consultants Ltd.

Davies, P. A. 1992 Aspects of flow visualisation and density field monitoring of stratified flows. *Optics Lasers Engng* **16**, 311–335.

Fincham, A. M., Maxworthy, T. & Spedding, G. R. 1996 Energy dissipation and vortex structure in freely decaying, stratified grid turbulence. *Dyn. Atmos. Oceans* **23**, 155–169.

Flór, J. B. & Heijst, G. J. F. van 1996 Stable and unstable monopolar vortices in a stratified fluid. *J. Fluid Mech.* **311**, 257–287.

Flór, J. B., Heijst, G. J. F. van & Delfos, R. 1995 Decay of dipolar vortex structures in a stratified fluid. *Phys. Fluids* **7**, 374–383.

Fortuin, J. M. H. 1960 Theory and application of two supplementary methods of constructing density gradient columns. *J. Polymer Sci.* **44**, 505–515.

Hartman, R. J. & Lewis, H. W. 1972 Wake collapse in a stratified fluid: linear treatment. *J. Fluid Mech.* **51**, 613–618.

Kloosterziel, R. C. 1990 On the large-time asymptotics of the diffusion equation on infinite domains. *J. Engng Maths* **24**, 213–236.

Lighthill, J. 1978 *Waves in Fluids.* Cambridge University Press.

Lighthill, J. 1996 Internal waves and related initial-value problems. *Dyn. Atmos. Oceans* **23**, 3–17.

Lilly, D. K. 1983 Stratified turbulence and the mesoscale variability of the atmosphere. *J. Atmos. Sci.* **40**, 749–761.

McWilliams, J. C. 1984 The emergence of isolated coherent vortices in turbulent flow. *J. Fluid Mech.* **146**, 21–43.

Oberhettinger, F. 1972 *Tables of Bessel Transforms.* Springer.

Oster, G. & Yamamoto, M. 1963 Density gradient techniques. *Chem. Rev.* **63**, 257–268.

Pao, H.-P. & Kao, T. W. 1977 Vortex structure in the wake of a sphere. *Phys. Fluids* **20**, 187–191.

Pedlosky, J. 1979 *Geophysical Fluid Dynamics.* Springer.

Riley, J. J., Metcalfe, R. W. & Weissman, M. A. 1981 Direct numerical simulations of homogeneous turbulence in density stratified fluids. *Proc. AIP Conf. Nonlinear Properties of Internal Waves*, (ed. B. J. West), pp. 79–112.

Schmidt, M. R., Beckers, M., Nielsen, A. H., Juul Rasmussen, J. & Heijst, G. J. F. van 1998 On the interaction between two oppositely signed, shielded, monopolar vortices. *Phys. Fluids* **10**, 3099–3110.

Spedding, G. R., Browand, F. K. & Fincham, A. M. 1996 Turbulence, similarity scaling and vortex geometry in the wake of a towed sphere in a stably stratified fluid. *J. Fluid Mech.* **314**, 53–103.

Terez, D. & Knio, O. M. 1998 Numerical study of the collapse of an axisymmetric mixed region in a pycnocline. *Phys. Fluids* **10**, 1438–1448.

Trieling, R. R. & Heijst, G. J. F. van 1998 Decay of monopolar vortices in a stratified fluid. *Fluid Dyn. Res.* **23**, 27–43.

Verzicco, R. & Orlandi, P. 1996 A finite-difference scheme for three-dimensional incompressible flows in cylindrical coordinates. *J. Comput. Phys.* **123**, 402–414.

Wu, J. 1969 Mixed region collapse with internal wave generation in a density-stratified medium. *J. Fluid Mech.* **35**, 531–544.